



ELSEVIER

Physica D 133 (1999) 371–389

PHYSICA D

www.elsevier.com/locate/physd

## Size and heterogeneity effects on the strength of fibrous composites

Sivasambu Mahesh<sup>a,\*</sup>, Irene J. Beyerlein<sup>b</sup>, S. Leigh Phoenix<sup>a</sup>

<sup>a</sup> Department of Theoretical and Applied Mechanics, 212 Kimball Hall, Cornell University, Ithaca, NY 14853, USA

<sup>b</sup> Materials Science and Technology Division, MS G755, Los Alamos National Laboratory, Los Alamos, NM 87545, USA

### Abstract

Probabilistic fiber composite strength distributions and size scalings depend heavily on both the stress redistribution mechanism around broken fibers and properties of the fiber strength distribution. In this study we perform large scale Monte Carlo simulations to study the fracture process in a fiber composite material in which fibers are arranged in parallel in a hexagonal array and their strengths are given by a two-parameter Weibull distribution function. To calculate the stress redistribution due to several broken fibers, a realistic 3D shear-lag theory is applied to rhombus-shaped domains with periodic boundary conditions. Empirical composite strength distributions are generated from several hundred Monte Carlo replications, particularly for much lower values of fiber Weibull modulus  $\gamma$ , and larger composite sizes than studied previously. Despite the localized stress enhancements due to fiber failures, predicted by the shear-lag model, composite response displays a transition to equal load sharing like behavior for approximately  $\gamma \leq 1$ . Accordingly, the results reveal distinct alterations in size effect, failure mode, and weak-link scaling behavior, associated with a transition from *stress-driven* to fiber *strength-driven* breakdown. ©1999 Elsevier Science B.V. All rights reserved.

**Keywords:** Composite materials; Computational mechanics; Probability; Tensile strength; Hexagonal packing

### 1. Introduction

Continuous fiber composites have much potential for high performance under high temperature and high loading conditions. A variety of material systems for such composites have been developed for a variety of specific applications, such as carbon fiber polymer matrix composites used for several structural civil engineering and automotive applications and ceramic fiber–ceramic matrix composites used in high temperature corrosive environments as say, gas turbine engine components.

Fiber composites have a reputation for being superior in their stiffness, strength, and creep resistance but reliability is difficult to predict, compared to their isotropic counterparts. Unlike composite elastic constants, there exists a substantial variation in the maximum mechanical stress which can be sustained (under compression, tension, fatigue and long term creep). Therefore, predicting composite strength naturally lends itself to reliability (or failure

\* Corresponding author. Tel.: +1-505-665-6662; fax: +1-505-665-2992

E-mail address: sm95@cornell.edu (S. Mahesh)

<sup>1</sup> Present address: MST-CMS, MS K765, Los Alamos National Laboratory, Los Alamos, NM 87545, USA.

probability) analyses. So, for example, in high reliability composite designs, engineers strive to minimize failure probabilities (e.g. one failure out of  $10^6$  components) for a given lifetime (e.g. 50,000 h) with knowledge of the material microstructure and phase properties. Requirements for efficient design are therefore not only the accurate knowledge of composite average strength, but also a characterization of the probability distribution for composite strength. As composite strength varies with composite size (length and width), interface properties, and the statistical properties of the fiber, it is of considerable interest to determine their influence on composite strength.

For fiber composites of interest here, variability in the fiber strength is primarily responsible for the variability and size effects observed in composite strength. High strength and brittle fibers, such as non-oxide (e.g., SiC), ceramic oxide (e.g., alumina), and graphite fibers typically exhibit large variability in strength due to flaws of varying severity that are randomly distributed along their lengths. The two-parameter Weibull model [1] has typically been the empirical statistical distribution of choice among both experimentalist and theoreticians, for representing fiber strength. Though not addressed in this paper, the variation in the tensile strength of a unidirectional composite may also be enhanced by the variation in its geometry, such as length and number of fibers, constituent material properties, including interface, and also features of its microstructure (fiber volume fraction, fiber arrangement etc.).

In statistical analytical modeling approaches, it has proven a formidable task to model composite failure evolution without resorting to major simplifications, particularly on the scheme for redistributing stress from broken fibers onto intact fibers. One such simplification is to assume that stresses borne by broken fibers are transferred according to a simple rule, such as the equal load sharing (ELS) or local load sharing (LLS) rule. In ELS, all the intact fibers share the applied stress equally and thus equally carry the loads lost from broken fibers, but in LLS, only the immediate unbroken neighbors carry these lost loads, thus causing more severe overloads than those that occur by ELS. The classic asymptotic fiber bundle strength distribution model as pioneered by Daniels [2] considers a dry bundle of fibers (with no matrix) which assumes ELS among non-failed fibers. Under LLS or similar localized stress transfer, a common approach has been to proceed with certain assumptions on the fiber fracture sequences and their probabilities as for example in, Zweben [3] and Zweben and Rosen [4], Argon ([5], p.79), ([6], p.153), Batdorf [7], and the chain of bundles probability models of Harlow and Phoenix [8,9]. In particular, the chain of bundles model, wherein fiber bundles are arranged in series, has enjoyed much success since its development with extensions to time-dependent fiber failure, matrix creep, 3D hexagonally-arranged fibers, and hybrid fiber composites [10–13]. Despite the use of idealized rules, these models have provided much insight into the characteristics and size effects in composite distributions as a function of fiber strength. However, stress redistribution in actual composites falls somewhere in between LLS and ELS, since a substantial portion of the stress is also redistributed to other non-failed neighbors. More realistic micromechanical models, like the one used in this study directly account for fiber and matrix deformation. They also allow for the possibility of matrix cracking, localized matrix plasticity, and interfacial debonding and thus, can potentially be more useful in design. Most notable amongst these is due to Hedgepeth and Van Dyke [14]. Monette and Anderson [15] give an energy based failure criterion for square and triangular lattices.

With this in mind, several researchers have used Monte Carlo simulations to study fiber composite breakdown incorporating finite difference, finite element methods, influence function techniques [16–18], and lattice Green's functions [19], for stress redistribution around fiber breaks. Examples of such studies, particularly using a Weibull distribution for assigning random strengths to fiber elements, include Manders et al. [20], Ochiai and Osamura [21], Goda and Phoenix [22], Baxenvanakis et al. [23], and Beyerlein and Phoenix [24,25] for simulations of 2D planar composites and Ibnabdeljalil and Curtin [26,27] and Landis et al. [28] for simulations of 3D composites with regular square packing. Both Beyerlein and Phoenix [24,25] and Ibnabdeljalil and Curtin [26,27] generated composite strength distributions for both pristine and notched composites and developed analytical probability models for the distribution of composite strength, which achieved good agreement with simulation results. However, in virtually all these studies, especially ones involving 3D composites, the regimes of extreme heterogeneity in fiber strength and large numbers of fibers could not be simulated within a reasonable amount of time.

Several network or lattice models of failure of heterogeneous materials have been developed to treat conductivity and dielectric *breakdown* in networks and catastrophic failure of elastic lattices, particularly in connection with percolation theory. Most of these studies deal with discrete 0 – 1 models for strength rather than continuous distributions, such as the Weibull distribution used here. Network sizes of  $200 \times 200$  are common with these 0 – 1 models but not with composite materials with Weibull fibers. However a majority of the proposed size scalings (logarithmic or power-law) from percolation theory and strength distributions have not been observed in simulations of breakdown and are often based on limited size networks [29–33]. Nonetheless for fiber bundles, such results are highly dependent on the stress redistribution model and distribution for fiber strength. Thus, in the present study, we employ a realistic elastic 3D computational technique for stress redistribution and compare the results to those assuming the more idealized ELS rule.

Li and Duxbury [31], Duxbury and Leath [32] and Duxbury [33] were the first to show repeatedly that the standard percolation models do not work in describing breakdown in lattice systems. As will be seen later, composite failure can occur when a non-percolating fiber break cluster reaches a certain critical size. On the other hand, formation of a percolating cluster does not imply composite failure with probability 1 either.

There are some common results of both analytical and computational work on fiber composites using LLS or numerical techniques for stress redistribution and  $\gamma \geq 3$ . As one would expect, as the mean fiber strength increases, the mean composite strength increases accordingly, and remains less than that of the fiber. Also, the variation in fiber strength appears to play an important and peculiar role. Firstly, it is the spread in fiber strengths which leads to multiple break accumulation prior to failure and in turn, suppresses the simple Weibull weak link size scaling of simple flaws seen in the fracture of monolithic ceramics and brittle fibers. Consequently, the composite strength distribution is non-Weibull, even when generated from controlled Monte Carlo simulations beginning with Weibull fibers. Secondly, when variation in fiber strength is above a certain threshold, fiber breaks occur at the weaker flaw sites and tend to be widely dispersed. Also the composite is insensitive to initial flaws. However when stress concentrations dominate, fiber breaks tend to cluster and localize, and composite strength is extremely sensitive to the size and location of preexisting flaws. Indeed, most composite systems studied in previous works display a complex interplay between the two factors. The objective of this work is to study the two extreme situations, *stress dominance* (in low fiber strength variability systems) and *fiber strength dominance* (in high fiber strength variability systems) and relate their resulting failure modes to composite strength and size effects.

The remainder of the paper is now outlined. We begin by describing the two primary components of the fiber composite model, the probabilistic fiber model and the two stress redistribution models considered. Next we develop the computational algorithm of the Monte Carlo simulation and follow that with results on the influences of fiber properties, composite size, and the stress redistribution scheme on composite distribution.

## 2. Probabilistic fiber model

We consider an infinitely long unidirectional fiber composite consisting of aligned, linear elastic fibers. They are assumed to have equal cross-sectional area, length, and elastic properties and to be independent and identically distributed in strength. The composite is loaded in tension in the fiber direction with stress per fiber of  $x$ .

The statistical nature of brittle fibers is due to flaws of random strengths distributed randomly along the fiber length. As is observed experimentally for such fibers, we assume that the random strength of a fiber of length  $L$  follows a two-parameter Weibull [1] distribution,

$$\Pr[X \leq x] = 1 - \exp\left(-\frac{L}{L_0} \left(\frac{x}{x_0}\right)^\gamma\right), \quad (1)$$

where  $X$  is the random variable for fiber strength,  $\gamma$  is the shape parameter and  $x_0$  the scale parameter for a fiber of length  $L_0$ . Thus the mean fiber strength is given by  $\mu_f = x_0\Gamma(1 + (1/\gamma))$  and the variance,  $\sigma_f^2 = x_0^2\{\Gamma(1 + (2/\gamma)) - \Gamma^2(1 + (1/\gamma))\}$  which decreases with increasing  $\gamma$ . Thus,  $\gamma$  is a measure of the variability of the fiber strengths: fibers with smaller  $\gamma$  have larger strength variability and vice versa. The two statistical parameters,  $\gamma$  and  $x_0$ , can be readily obtained from laboratory static tensile tests on several fibers at a given gauge length  $L_0$  [34,35] or by single fiber fragmentation tests [36]. The common values for  $\gamma$  of pristine fibers range from 2 to 20. However, fiber flaws inevitably introduced in composite fabrication tend to lower  $\gamma$  of the in-situ fibers [35]. Also, low  $\gamma$  composites may be used as a surrogate for investigating effects of discontinuous fiber composites since upon initial loading a large number of distributed breaks tend to form.

Owing to the statistical nature of the fiber strengths, fibers in a composite do not necessarily fail in regions of highest stress concentration. Also, many fiber breaks can accumulate before a running, catastrophic crack is created. Therefore, the failure plane of the composite is, in general, a three-dimensional surface. However, in this study, we make the simplifying assumption that the fibers have a constant strength along their length and limit the failure surface to a 2D plane perpendicular to the fiber direction. This assumption removes the longitudinal size effect of the composite, i.e.,  $L/L_0 = 1$  in (1).

With this restriction in place, we are able to simulate the failure process in composites with much smaller  $\gamma$  and much larger number of fibers than in previous studies. Also it becomes easier to isolate the effects of  $\gamma$  and number of fibers on composite strength. This also allows us to focus on the competition between stress concentrations in the composite (or stress dominance) and random fiber strength (or fiber strength dominance) to dominate the failure process and thereby gain insight for further analytical modeling.

We next discuss the fiber tensile stress calculation due to multiple in-plane fiber breaks.

### 3. Stress redistribution due to fiber breaks: two models

This section surveys two models that describe the redistribution of the stress dropped by an arbitrary collection of broken fibers on the surviving fibers. The first one considers a fiber composite consisting of aligned, hexagonally-packed fibers embedded in a low volume fraction of linearly elastic matrix, which is well-bonded to the fibers. This numerical stress field model realistically accounts for the elastic deformation of the fiber and matrix phases and interactions between multiple breaks. It is essentially the shear-lag model developed by Hedgepeth and Van Dyke [14] for an infinite hexagonal array of fibers applied to a finite set of fibers with periodic boundary conditions. In what follows, we will refer to the original Hedgepeth and Van Dyke model as the HVD model and to our periodic version of their model as the HVDP model.

Several other stress redistribution schemes have been proposed which are extremely idealized, requiring very little computational effort to simulate. The second stress model we use is one such idealization, viz., the ELS model, for a loose bundle of fibers. This simple model was selected for comparison with HVDP since accurate relations for composite strength distribution for an asymptotically large ELS composite are known [2]. Despite the significant differences between these two models of stress redistribution, we will find that at small  $\gamma \leq 1$ , the failure behavior of the composite turns out to be very similar. Both models are briefly discussed below.

#### 3.1. HVD shear-lag model

The HVD model is more realistic than the ELS model for a composite as it accounts for the effect of the elastic deformation of the matrix and the fibers on the redistribution of tensile stress. One assumption in this model is that the tensile stress in the matrix is negligible. The matrix is assumed to be in a state of pure shear, the shear stress

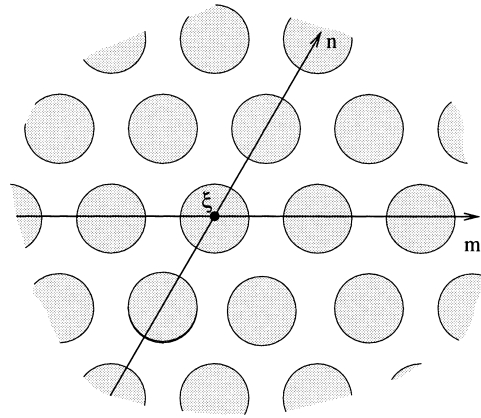


Fig. 1. The  $m$ – $n$ – $\xi$  coordinate system for fiber locations in model fiber composite.  $m$  and  $n$  include a  $60^\circ$  angle and the  $\xi$  direction is perpendicular to the plane of the paper.

being directly proportional to the relative displacement of the two flanking fibers. This assumption is appropriate for composites, wherein  $E_f V_f \gg E_m V_m$  where  $E_f$  and  $V_f$  are the stiffness and volume fraction of the fiber and  $E_m$  and  $V_m$  are the corresponding quantities of the matrix.

The stress redistribution produced by this model is long range and diffuse. When a fiber breaks, the stress dropped by the fiber is transmitted through shear in the matrix to significantly overstress the surrounding intact fibers over a 3D region whose size depends on the number of breaks and their configuration. Along the fiber, the stress at the fiber break drops to zero but builds up to the remotely applied fiber stress  $x$  along the fiber direction due to shearing in the matrix.

The HVD model also agrees with continuum theories when applied to infinite fiber arrays with large numbers of failed fibers. For the benchmark case of a straight crack in an elastic, anisotropic plate, the 2D shear-lag model [37] predicts stress distributions in excellent agreement with continuum fracture mechanics [16]. Also these shear-lag models of Hedgepeth [37] and Hedgepeth and Van Dyke [14] have been extended to treat other types of shear deformation in the matrix (e.g. plastic, viscoelastic, frictional) alterations which greatly influence fiber stress redistribution (see for example, Beyerlein et al. [17,18]).

We now present the HVD solution when applied to hexagonal arrays. Following Hedgepeth and Van Dyke [14], we set up an  $m$ – $n$ – $\xi$  coordinate system as shown in Fig. 1 and use it to identify fiber positions. We use  $\xi$  as the normalized coordinate and  $z$  as the physical coordinate in the fiber direction with their relation being  $\xi = z\sqrt{G_m h / E_f A d}$ , where  $A$  is the fiber cross sectional area,  $d$  is the surface–surface distance between two neighboring fibers and  $G_m h$  is the effective matrix shear stiffness.

The stress concentration at the position  $(m, n, \xi)$  due to a fiber break at  $(m_0, n_0, \xi_0)$  is given by

$$K_{(m,n,\xi),(m_0,n_0,\xi_0)} = 1 + u_0 \int_{-\pi}^{\pi} d\theta \int_{-\pi}^{\pi} d\phi \omega \exp(-\omega|\xi - \xi_0|) \cos((m - m_0)\theta + (n - n_0)\phi), \tag{2}$$

where

$$\omega = \sqrt{2(3 - \cos(\theta) - \cos(\phi) - \cos(\theta - \phi))} \tag{3}$$

and  $u_0$  is

$$u_0 = \frac{1}{\int_{-\pi}^{\pi} d\theta \int_{-\pi}^{\pi} d\phi \omega} \approx 0.0107, \tag{4}$$

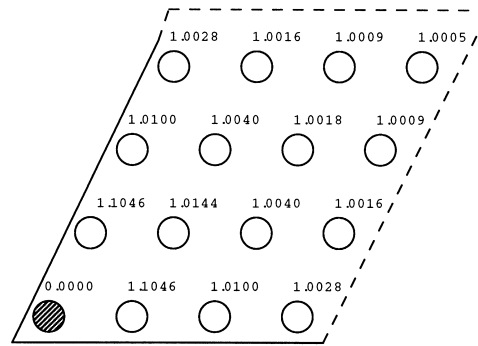


Fig. 2. HVDP stress concentrations near a single break in a  $30 \times 30$  periodic patch. The hatched fiber is broken. For this patch, the ELS stress concentration on the surviving fibers is  $1 + 1/899 \approx 1.0011$ .

which is chosen to satisfy the traction free boundary condition at the fiber break. It also turns out that  $2u_0$  is the normalized opening displacement of the single fiber break. Note that the in-plane stress concentrations, (when  $\xi - \xi_0 = 0$ ) in (2), are independent of fiber and matrix properties. In our simulations, all fiber breaks occur on the  $\xi = 0$  plane.

### 3.2. HVDP shear-lag model

This section describes the geometry of the finite periodic patches used in this study. We want the shape of the finite patch be such that (i) it would allow for periodic repetitions in the  $m$  and  $n$  directions and (ii) the geometry yields rotational and translational invariance in the stress field produced by a single break. Rhombus-shaped patches satisfy these requirements. (Hexagonal patches do not meet criterion (ii) above.) We will refer to the number of fibers in a patch as the patch size,  $s$ . More commonly, we will specify rhombus patches by giving the patch dimensions in terms of the number of fibers on each side (for instance, a  $30 \times 30$  patch has 30 fibers on each side and has size  $s = 900$ ). The method of computation of the single break solution in a periodic patch with a hexagonal lattice is similar to that given in Landis et al. [28] for a square lattice.

In Fig. 2 we show the stress concentrations on fibers around a single break in a  $30 \times 30$  periodic patch as predicted by the HVDP model. In an infinite composite, the stress concentrations are known to decay proportional to  $\rho^{-3}$ , where  $\rho$  is the radial, in-plane distance from the fiber break [38]. In comparison, under ELS, the stress concentration in all these fibers would only be  $1 + (1/(900 - 1)) \approx 1.0011$ . As shown in Fig. 2, the HVDP stress concentrations, within the first four fibers around the break, are higher than this ELS value.

The general influence function technique used to solve for the 3D stress field around multiple fiber breaks consists of two steps. First, the solution for the stress redistribution due to an isolated break in a periodic patch of size  $s$  (HVDP) or a patch of infinite extent (HVD) is determined. Then, the multi-break solution is obtained as a weighted superposition of the unit break solutions with the weights determined such that the stress field satisfies the traction free boundary condition at all fiber breaks. The power of these influence function techniques is that the computation time depends on the number of breaks rather than the volume or number of fibers in the composite.

The HVD model was originally developed to handle fibers all lying within the same cross-sectional plane. Later, the fundamental framework was altered to calculate stress redistributions due to out-of-plane breaks [39]. Therefore, the HVDP can treat out-of-plane breaks as well with no increase in computation time. For details on the general method of solution, we refer the reader to Beyerlein et al. [16] for 2D and Landis et al. [28] for 3D.

### 3.3. Equal load sharing (ELS) model

In the ELS model, the stress dropped by a broken fiber or fibers is equally distributed among the intact fibers. That is, if there are  $r$  fiber breaks in a bundle of  $s$  fibers, the in-plane stress concentration (ratio of fiber stress to far field applied stress  $x$ ) on each of the surviving fibers is

$$K_r = \frac{s}{s-r}. \quad (5)$$

In this model, the relative positions of the broken fibers are irrelevant as well as fiber arrangement, and there is no localization of stress concentrations. The only random quantity that governs the probability of failure at each time is the *number* of fiber breaks at the previous time. ELS is a realistic model for a loose bundle of fibers (without matrix in between) and an approximate model for fiber–matrix composites, wherein the shear strength of the interface or friction between the fibers is negligible, i.e., it is much less than  $(1/2)\sqrt{G_m/E_f}$  times the average fiber strength [40]. Here,  $G_m$  and  $E_f$  are the shear modulus of the matrix and tensile modulus of the fiber respectively.

Under ELS, Daniels [2] showed that the strength of asymptotically large loose bundles is normally distributed, irrespective of the form and properties of the fiber strength distribution. According to the Daniels bundle model, for Weibull strength fibers following (1), the mean of the bundle strength is

$$\mu = sx_0c^c e^{-c} \quad (6)$$

and the standard deviation

$$\sigma = x_0c^c \sqrt{se^{-c}(1-e^{-c})}, \quad (7)$$

where

$$c = \frac{1}{\gamma}. \quad (8)$$

In general, given any configuration of breaks, the differences in the stress concentrations predicted by ELS and HVDP diminish as the bundle size  $s$  decreases. Despite the significant differences between these two models of stress redistribution, we will find that at small  $\gamma$ , the failure behavior of the composite turns out to be very similar. Where the above formulae are given for the entire composite, in comparison of the ELS model simulations with those of the HVDP simulations, we shall normalize all strengths by the number of fibers in the composite.

## 4. Monte Carlo simulation of the failure process

Before detailing the simulation procedure itself, we motivate the need for such a study by showing the infeasibility of direct calculation of the probability of failure of a HVDP composite. Consider a rhombus-shaped patch of  $s$  hexagonally-arranged Weibull fibers loaded at  $\xi = \pm\infty$  with stress per fiber  $x$  (i.e., the total stress applied to the composite patch is  $sx$ ). Consider the situation in which  $x$  is instantaneously applied to the composite and the progression of fiber breaks in “time increments” is monitored. This stress  $x$  first fails those fibers that have strengths smaller than  $x$  (at time 1). The load dropped by these fibers is now redistributed among the intact fibers according to either the ELS or the HVDP model. This overload may cause more fiber failures (at time 2) which in turn overload yet another set of fibers beyond their strengths and fail them (at time 3) and so on. Failure must be achieved by time  $s$  (which is the number of fibers) or less for the composite strength to be less than the applied stress  $x$ . Though failures occur sequentially in time, this is still considered to be a static problem.

Let  $B_i = (b_{1i}, b_{2i}, \dots, b_{si})$ ,  $i = \{1, 2, 3, \dots, s\}$ , be a collection of random vectors, in which  $b_{ki} = 0$  or 1, when fiber  $k$  is broken or intact, respectively, at time  $i$ . Since failures are restricted to occur on one plane in both ELS and HVDP, the occurrence of additional breaks cannot reduce the stress on unbroken fibers. Therefore,  $\{B_i\}$  is Markov with state space  $[0, 1]^s$ . That is,

$$\Pr[B_{i+1} \in A | B_j, j = 1, 2, \dots, i] = \Pr[B_{i+1} \in A | B_i] \quad (9)$$

for  $i \in \{1, 2, \dots, s\}$  with a fixed applied stress  $x$ . Here  $A$  is any set of  $s$ -vectors of 0's and 1's and  $B_0 = \{0, 0, \dots, 0\}$ .

Thus the problem is essentially one of finding the transition probability from  $\{0\}^s$  to  $\{1\}^s$ . In order to compute the strength distribution of the composite exactly, one must first form the  $2^s \times 2^s$  transition matrix and then sum probabilities over all the paths leading from  $\{0\}^s$  to  $\{1\}^s$ . However, the number of ways of traversing the state space explodes as  $s^s$  rendering exact calculations of the composite strength distribution from the fiber strength distribution intractable.<sup>2</sup>

For this reason, we seek to find ways of reducing the size of the state space. Our approach is to learn from the Monte Carlo simulations what the *dominant paths* of failure are and to sum probabilities only over those failure paths. This investigation is a precursor to approximate probabilistic calculations for the strength distribution of fiber composites, especially at extremely low probabilities, and for size scaling laws. By simulations alone we cannot expect to reach low probability levels ( $10^{-6}$ ) for composite patches with a large number of fibers ( $10^6$ ), as in real materials, as the computation time will be prohibitively large.

We now describe the simulation algorithm. Fig. 3 shows the simulation flow-chart used for both the ELS and HVDP cases. First a value of  $\gamma$  and a patch size,  $s$ , are fixed and 500 simulations performed. In each of these simulations, an independent and identically distributed sample of Weibull strengths are assigned to the  $s$  fibers in the patch. The patch is then stressed by a load applied at  $\pm\infty$  to fail at least one fiber in it. The stress dropped by the broken fiber(s) is(are) then redistributed among the surviving fibers using ELS or HVDP. Further failures due to this overload are then checked for, giving rise to two situations. If one or more fibers are overloaded, then these are broken and the stress redistribution is computed. If no such failures occur, the stress per fiber is increased so as to break at least one more fiber. The entire process is then repeated until all the fibers are broken. The minimum stress at which all the fibers are failed is the composite strength. From the 500 strengths for each set of  $\gamma$  and  $s$ , an empirical composite strength distribution is obtained. The failure mechanisms arising in different cases are also obtained. As we shall see, the dominant failure mechanism is one of fiber break clustering in the case of fibers with high  $\gamma (> 1)$  and one of dispersed breaking in the case of low  $\gamma (\leq 1)$ .

<sup>2</sup> This also includes paths of zero probability. The paths with nonzero transition probability from  $\{0\}^s$  to  $\{1\}^s$  are the ones wherein (i) broken fibers do not heal themselves and (ii) in all stages or times prior to failure, at least one break must occur. The number of these paths to failure may be calculated as

$$\widehat{N}_s = \sum_{m=1}^s N_m, \quad (10)$$

where  $N_m$  is the number of paths with nonzero probability from  $\{0\}^s$  to  $\{1\}^s$  in exactly  $m$  times and is given by the recursion

$$N_m = m^s - \sum_{j=1}^m \binom{m}{j} N_{m-j} \quad (11)$$

with

$$N_0 = 0. \quad (12)$$

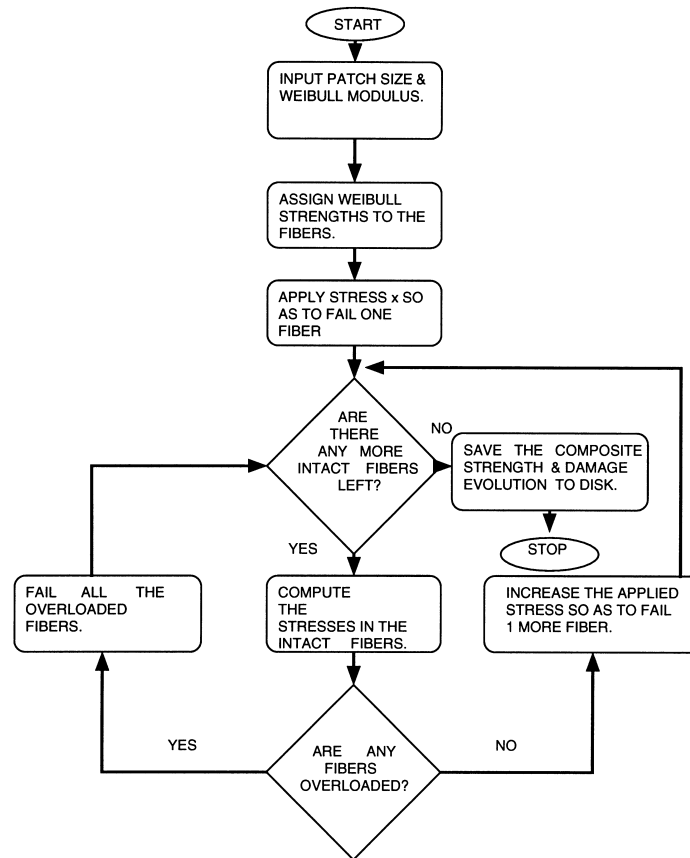


Fig. 3. The Monte Carlo simulation algorithm.

## 5. Monte Carlo simulation results

This section presents the empirical strength distributions obtained by the Monte Carlo simulations of composites consisting of different numbers of fibers,  $s$  and fiber shape parameter,  $\gamma$ . Specifically, simulations for  $s = 15 \times 15$ ,  $25 \times 25$ ,  $30 \times 30$ , and  $50 \times 50$  were executed. For each of the first three sizes, 500 simulations were run for cases  $\gamma = 1/2, 2/3, 1, 3, 5$  and 10. For  $s = 50 \times 50$ , however, only 100 simulations were run for  $\gamma = 1/2$  and  $\gamma = 10$  owing to computation time constraints.

In general, the empirical strength distributions from the HVDP simulations are not consistently either Weibull or normal. In agreement with Daniels' theory, the ELS simulations are consistently normal. In comparing the HVDP results to the ELS results, we are motivated by the normality of the asymptotic ELS strength distributions to plot the strengths on normal probability paper. This is a plot of the standard normal score  $z_i$  versus the associated ranked composite strength  $x_{(i)}$ , where  $i = 1, \dots, 500$ . On this probability paper, a normal distribution plots as a straight line with the mean  $\bar{x}$  given by the  $x$ -intercept and the standard deviation  $\sigma$  given by the reciprocal of the slope.

### 5.1. Weibull fiber modulus $\gamma$ effect

Fig. 4 shows the effect of  $\gamma$  on the distribution of composite strength normalized by  $s\mu_f$  for a  $30 \times 30$  patch using HVDP and ELS stress redistribution. (Recall  $s$  is the number of fibers in the composite patch and  $\mu_f$  the mean fiber

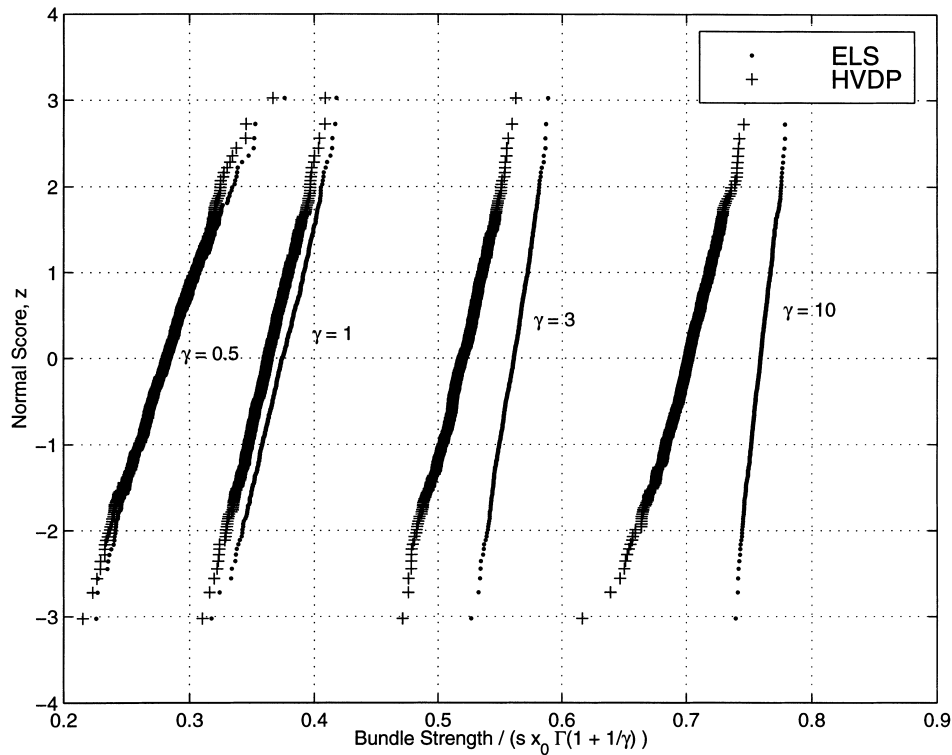


Fig. 4. Effect of the fiber Weibull modulus  $\gamma$  on the strength distribution of a  $30 \times 30$  patch on normal probability paper.

strength.) If plotted with no fiber strength normalization or against fiber strength normalized with just  $sx_0$ , it will be seen that both the ELS and HVDP distributions achieve a minimum mean strength approximately around  $\gamma = 1$  (or when the fiber strength follows an exponential distribution). In other words, for  $\gamma > 1$  the composite mean strength increases with  $\gamma$  and for  $\gamma \leq 1$ , it increases as  $\gamma$  decreases. The standard deviation increases monotonically with decreasing  $\gamma$  for both HVDP and ELS.

As shown, the differences in the ELS and HVDP strength distributions diminish as  $\gamma$  decreases, though the ELS composites are always stronger. However for  $1/2 \leq \gamma \leq 1$ , we observe that this trend is not monotonic. That is, there is a value of  $\gamma$ , not always equal to  $1/2$ , at which the difference between the ELS and HVDP composite is the least. This value of  $\gamma$  also depends on composite size. For instance, in the  $15 \times 15$  and  $25 \times 25$  composites, the difference is the least for  $\gamma = 2/3$  whereas for a  $30 \times 30$  patch, the difference is the least for  $\gamma = 1/2$ . In the limiting case of  $\gamma = 0$ , the difference between ELS and HVDP would vanish.

## 5.2. Failure patterns

Many of these general trends in the strength distribution with  $\gamma$  can be explained by studying patterns of fiber break accumulation prior to failure. Fig. 5 (a1) and (a2) show typical fiber break patterns in a  $10 \times 10$  periodic patch of a lower tail (weak) and upper tail (strong) HVDP composite, respectively, when  $\gamma = 10$ . These figures capture the failure pattern at a far field stress *just under* the composite strength. That is, for any far field stress exceeding this stress, all the remaining fibers in the composite would fail. Fig. 5 (b1) and (b2) make the same comparison for two  $\gamma = 5$  fiber composite specimens as do Fig. 5 (c1) and (c2) for  $\gamma = 1/2$  lower and upper tail specimen.

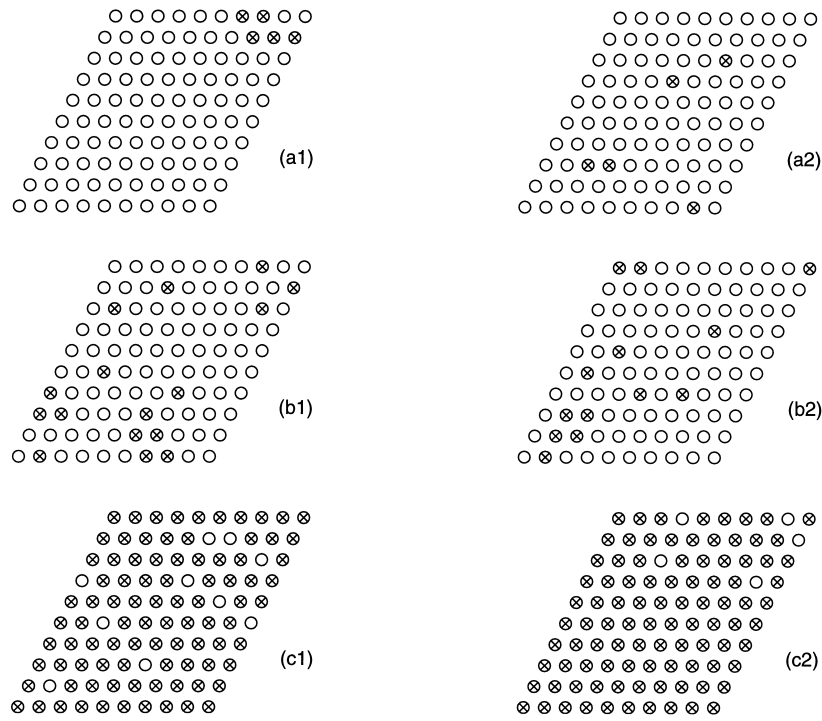


Fig. 5. Failure patterns in a  $10 \times 10$  composite patch. (a1) and (a2) are  $\gamma = 10$  lower and upper tail specimens respectively, (b1) and (b2) are  $\gamma = 5$  lower and upper tail specimen respectively, and (c1) and (c2) are  $\gamma = 1/2$  lower and upper tails respectively. Open circles denote intact fibers and circles with a “x” in them denote broken fibers.

As shown, the failure configurations at incipient failure are drastically different for  $\gamma = 1/2$  and  $\gamma = 10$ . Some qualitative conclusions may be arrived at from these figures. An immediate observation is that for  $\gamma = 10$ ,  $\gamma = 5$  and similarly for other high  $\gamma (\geq 3)$ , failure is due to clustering of a few breaks and catastrophic growth of a small and tight *critical cluster*. (We shall refer the collection of neighboring breaks which initiates failure in all remaining intact fibers without further increases in stress as the critical cluster.) On the other hand, in the case of  $\gamma = 1/2$ , and similarly for other low  $\gamma (\leq 1)$ , clustering of breaks does not occur. Instead, fiber breaks are formed in a very disperse manner. In this case, the critical cluster is not as easily distinguishable from the other clusters and is rather large and dispersed. These observations are to be expected, since when  $\gamma \geq 3$  or there is a relatively small spread among fiber strengths, the intact neighbors are likely to have strengths only slightly greater than the failed fiber. Consequently, the overload due to the failure of a fiber is very likely to cause additional failures in the adjacent intact neighbors. Thus for HVDP composites, when  $\gamma > 1$ , damage accumulation is *stress concentration driven*.

Starting at about  $\gamma = 2$  and particularly for  $\gamma \leq 1$ , the spread in fiber strength is larger and the intact neighbors of a failed fiber are more likely to be much too strong to fail without further increases in far field stress. At stresses small compared to the composite strength, the location of the new breaks remain widely dispersed, governed by the many relatively weaker fibers. Though clusters may form, relatively strong fibers can prevent further growth. In addition, widely dispersed breaks produce less tightly concentrated break clusters which in turn can further promote such random break patterns. Eventually catastrophic failure occurs when all the relatively strong fibers are left surviving. Also we believe that for this dispersed arrangement of fiber breaks, the stress enhancements in the surviving fibers are nearly equal, thereby giving the HVDP composite an “ELS-like” response for low  $\gamma \leq 1$ .

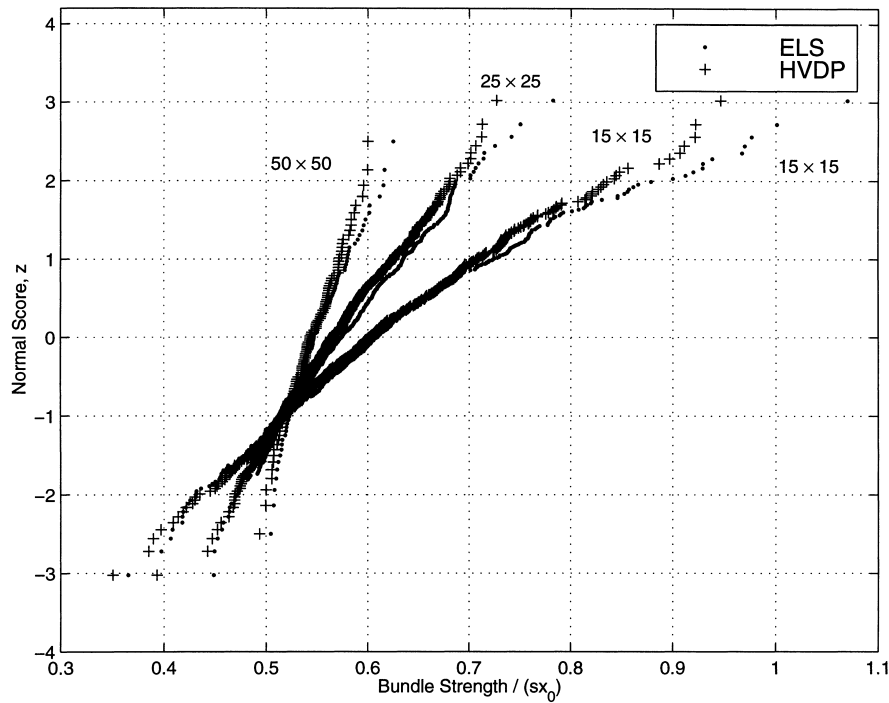


Fig. 6. Effect of the composite patch size  $s$  on composite strength with  $\gamma = 1/2$  Weibull fibers on normal probability paper.

Thus when  $\gamma \leq 1$ , damage accumulation is *strength driven*. Since the HVDP composites are consistently weaker than the ELS composites, it suggests that localized stress concentrations do still play a small role in damage accumulation.

Comparing the upper and lower tail specimen of the  $\gamma = 10$  case (Fig. 5(a1) and (a2)), the lower tail specimens show greater localization than the upper tail specimens. Though not illustrated, we find that the average critical clusters grow as  $\gamma$  decreases and given  $\gamma$ , the critical cluster is larger in a lower tail specimen than in an upper tail specimen for  $\gamma \geq 3$  for a fixed  $\gamma$ . Upper tail specimens are strong because they happen to have their weaker fibers dispersed. The lower tail specimens, on the other hand, are weak because they happen to have a region of weaker fibers failing at a low applied stress producing higher stress concentrations to further propagate the cluster. The upper and lower tail specimens of the  $\gamma = 1/2$  fiber composites are typical of the other  $\gamma \leq 1$  realizations and are not significantly different.

### 5.3. Size effect

Figs. 6 and 7 show the effect of patch size,  $s$  on composite strength for the  $\gamma = 1/2$  and  $\gamma = 10$  fiber composites, respectively. A common trend between these two values of  $\gamma$  and two models of stress transfer, HVDP and ELS, is that both the mean strength and the standard deviation decrease with increasing composite size. As seen from the failure patterns, it is the relatively weak fibers in the composite which initiate the failure process and in turn govern the strength of the composite. Larger composites contain a larger number of these weaker fibers. For the HVDP composites, these weaker fibers may also serve as potential nucleation sites from which fiber break clusters can grow. This provides one explanation as to why for fixed  $\gamma$ , the size effect is greater in the HVDP composites. The

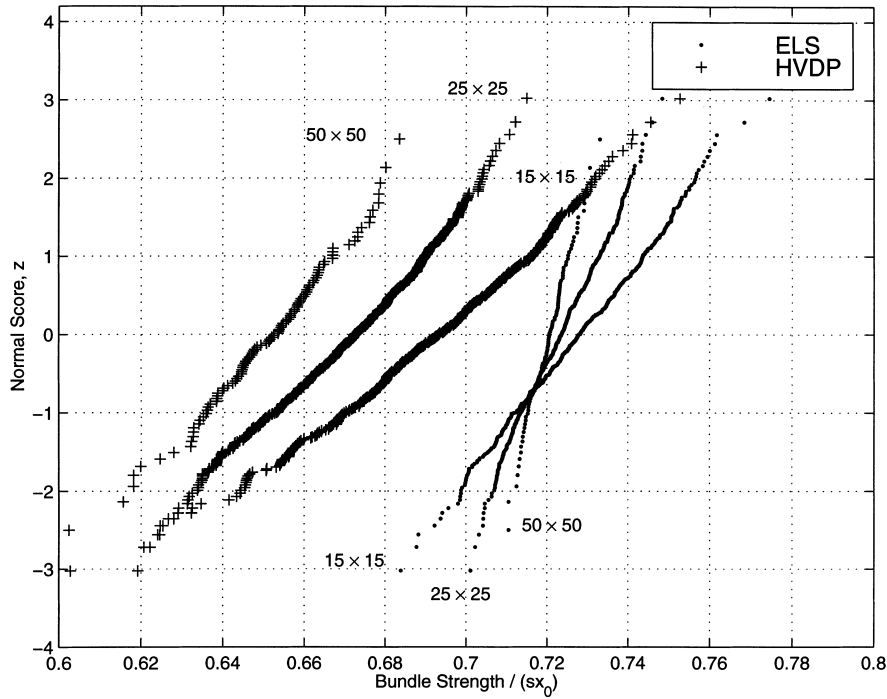


Fig. 7. Effect of the composite patch size  $s$  on composite strength with  $\gamma = 10$  Weibull fibers on normal probability paper.

variation in composite strength decreases with composite size as the failure process in larger composites involves more fiber breaks up to the composite strength. More breaks are involved since in both ELS and HVDP, the stress concentrations are lower as  $s$  increases for a given fiber break pattern.

Though not illustrated, note that these ELS bundles closely approach Daniels asymptotic result, as  $s$  increases and at a rate increasing in  $\gamma$ . For  $\gamma = 10$ , the normalized sample mean for the ELS  $50 \times 50$  size composite is  $\bar{x}/s x_0 = 0.7207$  compared to 0.7187 using Eq. (6). For  $\gamma = 1/2$ ,  $\bar{x}/s x_0$  for the ELS  $50 \times 50$  and  $100 \times 100$  size composites are 0.5511 and 0.5476, respectively, compared to 0.5413 using (6).

Figs. 6 and 7 reveal that the size effect is stronger for  $\gamma = 1/2$  than  $\gamma = 10$ , i.e. changes in mean and variation to changes in  $s$  is greater for  $\gamma = 1/2$ . In the  $\gamma = 1/2$  plot, we observe that the distributions for the three sizes cross over in the lower tail. Due to the increase in variability in composite strength as  $s$  decreases, the size effect is negative in the upper tail and positive in the lower tail. However for the sizes simulated and the probability range shown, composite distributions for  $\gamma = 10$  fibers do not cross. Based on the trends observed, these  $\gamma = 10$  distributions would cross at lower probability levels than simulated for the sizes considered. In addition, distributions with greater differences in size, say  $15 \times 15$  and  $200 \times 200$ , could be expected to cross within the displayed probability level. Comparing the HVDP and ELS cases, for the  $\gamma = 1/2$  composites, the HVDP distributions follow the shape of the ELS distributions for all sizes and also the size effects of the ELS composites quite well. However we speculate that for much larger HVDP composites the size effect will be distinct from that of ELS since ELS-like stress redistribution can only occur over a limited number of fibers in a cross section. For  $\gamma = 10$ , however, these two cases are drastically different, as typically observed in previous works.

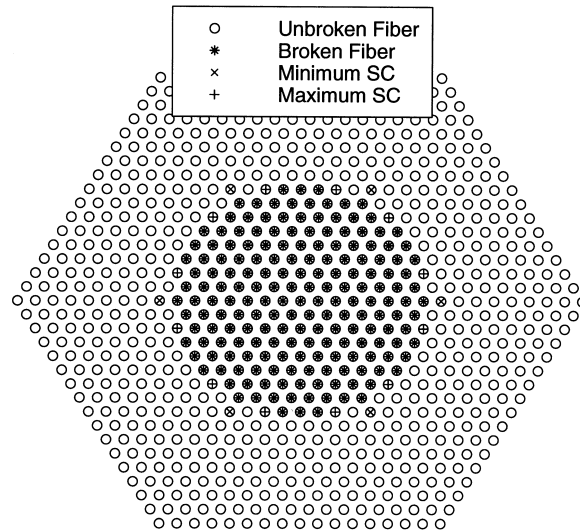


Fig. 8. A penny-shaped cluster of 187 breaks of radius  $R = 7$ .  $R$  is the maximum number of inter-fiber spacings from the central fiber to a peripheral fiber. For radii smaller than 7, the “penny shape” crack is actually hexagonal.

## 6. Modeling the failure process

### 6.1. Stress concentrations around a circular break cluster

As described in Section 3 the calculation of stresses in a HVDP composite with even a few fiber breaks is rather involved. In analytical probabilistic calculations, it is useful to have simple formulae for stress concentrations around fiber break clusters commonly observed in the failure patterns.

In the case of high  $\gamma (> 1)$  fiber composites, the critical cluster tends to form from one or more of the many clusters of breaks which evolve in the failure process. The critical clusters assume complex morphologies and especially for  $\gamma \leq 5$ , tend to be created from the coalescence of two or more smaller clusters. For simplicity, we first consider a tight penny-shaped cluster of breaks. We take a penny-shaped cluster to be one in which all the fibers whose centers lie a fixed distance  $R$  from the center of the fiber at  $(m, n) = (0, 0)$  are broken as depicted in Fig. 8. We assume that this penny-shaped fiber break cluster sits in an infinite hexagonal array and examine the stress concentrations around its perimeter. (Especially as  $R$  becomes large, this cluster can be reasonably identified as a penny-shaped crack.)

In what follows we shall refer to those intact fibers that have at least one failed neighbor that belongs to the penny shaped cluster as the *perimeter* of the cluster. Among other curves, Fig. 9 shows the maximum and minimum stress concentrations on the perimeter of the circular cluster calculated by the HVD model. It is found (see Fig. 9) that an excellent approximation for the minimum stress concentration on the perimeter is given by

$$K_{\min} = \sqrt{\frac{R}{\pi} + 1}, \quad (13)$$

where  $R$  is the number of fiber spacings along the radius of the penny-shaped cluster.

However, in modeling failure, one is interested in the maximum stress concentrations on the perimeter fibers. This is found to be

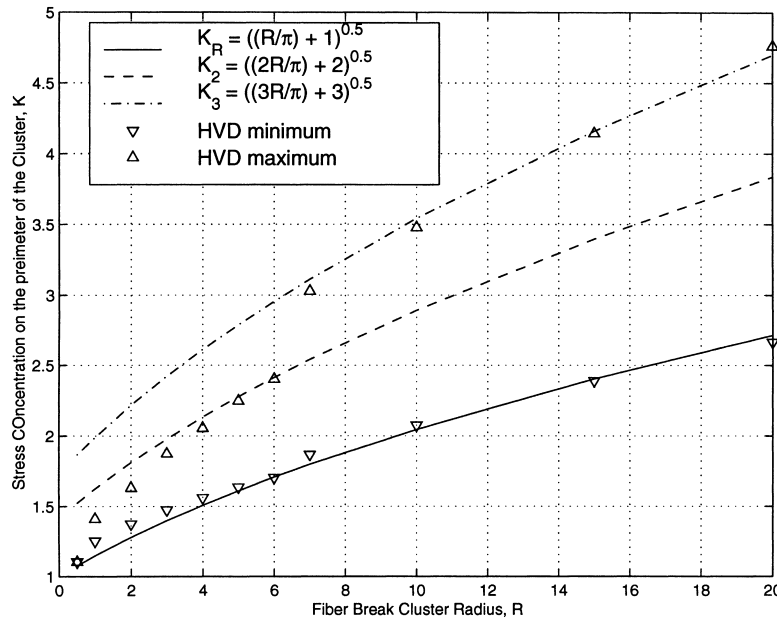


Fig. 9. Stress concentrations in the perimeter of a circular cluster of breaks of radius  $R$  embedded in an infinite patch.

$$K_{\max} = \begin{cases} \sqrt{2}\sqrt{\frac{R}{\pi}} + 1 = \sqrt{2}K_{\min} & \text{if } R \leq 6, \\ \sqrt{3}\sqrt{\frac{R}{\pi}} + 1 = \sqrt{3}K_{\min} & \text{if } R > 6. \end{cases} \quad (14)$$

Fig. 9 plots the two formulae for  $K_{\max}$  for all  $R$  in order to show their regions of validity. This plot refers to the two branches of  $K_{\max}$  as  $K_2$  and  $K_3$ . The physical explanation for the transition in the behavior of  $K_{\max}$  from  $R = 6$  to  $R = 7$  is based on the number broken neighbors surrounding an intact perimeter fiber. For penny-shaped clusters with  $R \leq 6$ , it is found that the cluster is hexagonal. Consequently, no perimeter fiber has more than two broken neighbors. However, as seen from Fig. 8, penny-shaped clusters with  $R \geq 7$  are circular and there exist perimeter fibers that have three broken neighbors. Since no fiber on the perimeter of a penny-shaped cluster can have more than three broken neighbors for any  $R$ , we believe that even for  $R > 20$  (values beyond those shown in Fig. 9) the maximum stress will be well approximated by (14).

Also based on classical linear elastic fracture mechanics results for an elastic, anisotropic continuum, the axial stresses decay proportional to  $\rho^{-1/2}$  in the near field from the edge of the penny-shaped crack. Fig. 10 shows the decay behavior of the average axial stress concentrations  $K_\rho$  with  $\rho/(d+h)$  for various crack sizes. As shown, the extent of the overstress region (or value of  $\rho/(d+h)$  where  $K_\rho = 1$ ) grows proportional to the size of the crack, but the decay behavior away from the crack perimeter is slower than  $\rho^{-1/2}$ . Therefore, the overstressed region grows faster than the crack-tip stress intensities with increases in  $R$ . Based on previous comparisons between an analogous 2D shear-lag model and linear elastic fracture mechanics [16], we speculate that as the crack size increases further, the decay behavior will approach  $\rho^{-1/2}$  over a larger crack-tip region. Also note the large drop in stress between the perimeter fibers and the next nearest fibers. This implies that it is more probable for the next fiber break to occur on the periphery of a growing cluster than elsewhere. In both Figs. 9 and 10, the circular cluster is assumed to be embedded in an infinite patch.

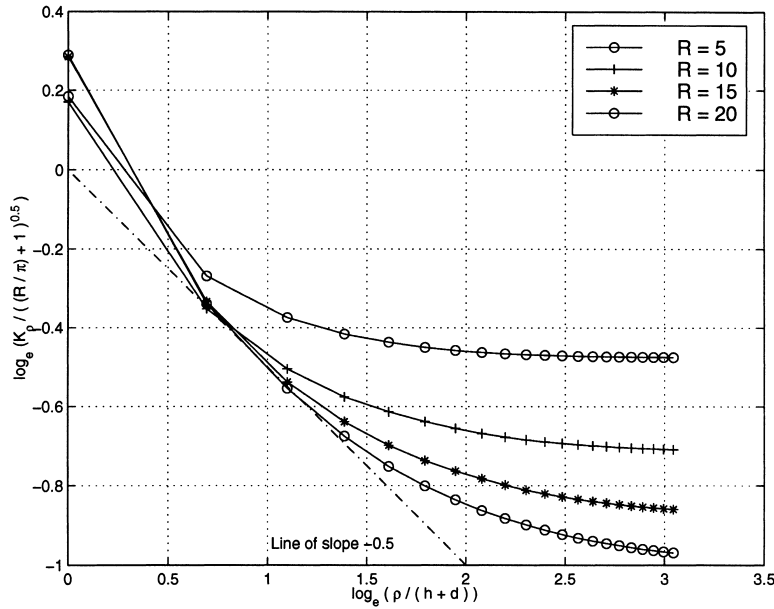


Fig. 10. Decay of the fiber stress concentration, normalized by (13) for different crack radii  $R$ , for distances  $\rho$  measured from the tip of the main diagonal of the crack. Recall  $d + h$  is the fiber-fiber center spacing.

6.2. Weakest link behavior

Following concepts introduced in Harlow and Phoenix [9] for LLS fiber bundles we ask the question: do the HVDP composites follow the weak-link scaling law and if so, for what values of  $\gamma$ . If  $G_s(x)$  is the strength distribution for a composite of size  $s$ , they find that there is a weak link characteristic probability distribution  $W_s(x) \approx W(x)$  such that

$$G_s(x) = 1 - (1 - W_s(x))^s \approx 1 - (1 - W(x))^s \approx 1 - \exp(-sW(x)). \tag{15}$$

In words, this relation implies that the probability of composite failure equals that of the weakest of  $s$  links, each following  $W(x)$  independent of  $s$ . In general, this function depends on the composite geometry, stress redistribution, and the statistical parameters of fiber strength. Also,  $W(x)$  is not a power in  $x$  so that  $G_s(x)$  is non-Weibull. For LLS fiber bundles and Weibull fibers with  $\gamma \geq 5$ ,  $W_s(x)$  is conjectured to converge to  $W(x)$  for  $s \geq 9$ . They find that ELS fiber bundles, however, do not follow weak-link scaling. Except for the simplest discrete fiber strength distribution,  $W(x)$  has not generally taken a straightforward analytical form, not even asymptotically.

Plotting the weakest link function,  $W_s(x)$  (Fig. 11), we find that for the probability ranges simulated ( $> 1/500$ ), all the different HVDP strength distributions for  $\gamma \geq 3$  collapse onto a single master curve, i.e.  $W_s(x) \rightarrow W(x)$  for  $\gamma \geq 3$ . As shown in Fig. 11,  $W(x)$  in these cases is not normal, and we find that it is also not Weibull. Admittedly, the weak-link scaling behavior in the  $\gamma < 3$  distributions shows evidence of breaking down in lower probability levels. For some  $\gamma$  between 1 and 3 however, weak-link scaling breaks down, especially in the lower tail. We speculate that this may be due to boundary effects, meaning the critical cluster size approaches the size of the rhombus-shaped patch.

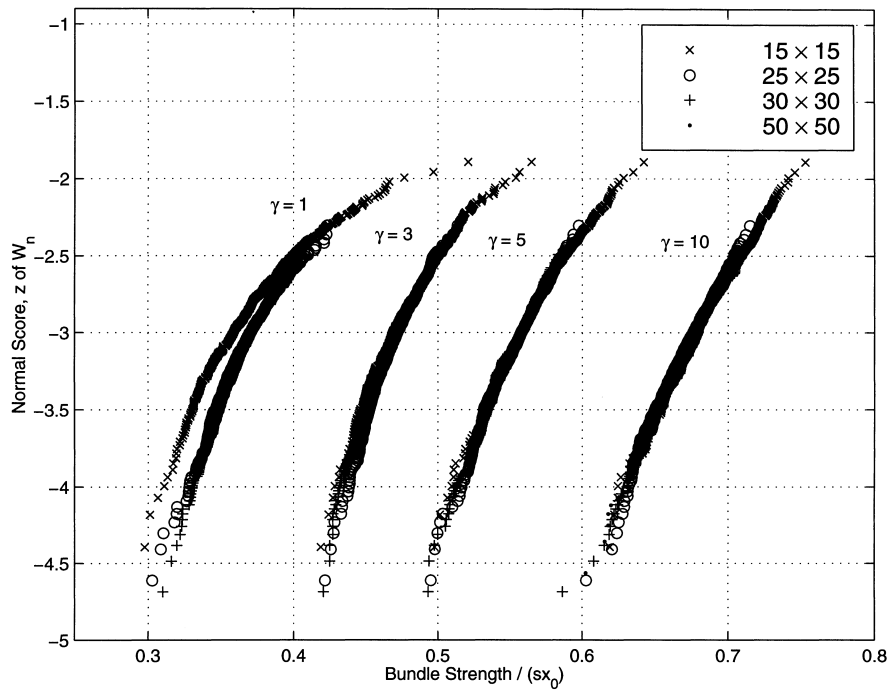


Fig. 11. Weakest link behavior in composites with fiber Weibull modulus  $\gamma \geq 1$  on normal probability paper.

### 6.3. Stress versus strength-driven failure

To summarize, as  $\gamma$  decreases, the composite variation decreases, size effect increases, and differences between the HVDP and ELS composites decrease. These results on the influences of  $\gamma$  and  $s$  brings us back to the issue of stress versus fiber strength-driven failure accumulation in the HVDP composites. Despite the fact that the HVDP stress redistribution model produces localized stress enhancements (see Figs. 2,9 and 10), the value of the fiber Weibull modulus  $\gamma$  plays a significant role in determining whether failure is stress or fiber strength-driven. When stress-driven in the case of  $\gamma > 1$ , overall composite behavior is not as sensitive to composite size  $s$ , as it is to localized stress concentrations. However, when fiber strength-driven, as in the case of  $\gamma \leq 1$ , the strength is sensitive to size or effectively, the *number* of weaker fibers in the composite (even if the percentage of weak fibers were to remain the same as  $s$  increases). Also when  $\gamma > 1$ , many large fiber break clusters tend to form at lower loads as  $\gamma$  decreases, which in this stress-driven regime, results in weaker overall composite strength. Lastly we find that stress-driven failure process follows a weak-link scaling, whereas the fiber strength-driven process does not. We speculate that this is because the cluster size in the latter case is greater than the size of the periodic patch.

## 7. Closing remarks

Indeed much of the cost of implementing such advanced materials into component design goes into developing a mature understanding and reliable predictive methods of its response in service. Clearly there is not enough time or money to determine the desired high reliability levels through real-time or even accelerated experimentation alone.

Computer simulation, complemented with experiments and analytical modeling, will certainly reduce the number of iterations and parameter spacing in the design cycle.

In the current investigation, we develop a large-scale 3D Monte Carlo simulation model to study the relationships between the statistical strength of the fiber and that of the parent composite for different sizes. The model employs a realistic shear-lag model producing diffuse, long range stress redistribution and accounting for interactions between multiple breaks. The scope of this study is to focus on competition between fiber stress concentrations (or stress dominance) and random fiber strength (or fiber strength dominance) to dominate the composite failure process and ultimately tensile strength.

To aid in this investigation, we limit failure to evolve within a 2D cross-sectional plane of the composite. In this way, we are able to simulate composites with much lower and much larger number of fibers than calculated in previous works. For fiber–matrix composites reinforced with extremely low  $\gamma$  fibers the failure mode is non-catastrophic. However, they fall short of being desirable structural materials due to the large spread in their strengths and small lower tail strengths relative to the  $\gamma > 1$  cases. Also as  $\gamma$  decreases, size effect in composite strength becomes stronger and particularly in the lower tail region, which is important in high reliability design, the size effect is positive (see Figs 6 and 7).

Understanding composite response in the regime of extreme heterogeneity brings further insight into the mechanisms driving stochastic failure for all ranges of fiber strength variation. From the subtle details of these simulations, we can investigate the dominant breaking sequences which lead to failure. Probabilistic calculations for composite strength based on number of fibers and properties of statistical fiber strength are currently being pursued in light of these results.

## Acknowledgements

IJB and SM would like to express their gratitude for the support and hospitality provided by the Center for Materials Science, Los Alamos National Laboratory, through a J.R. Oppenheimer Fellowship and a graduate research assistantship, respectively. SLP was supported by NSF CMS-9800413.

## References

- [1] W. Weibull, *J. Appl. Mech.* 18 (1951) 293.
- [2] H.E. Daniels, *Proc. R. Soc. Lond. A* 183 (1945) 405.
- [3] C. Zweben, *AIAA J.* 6 (1968) 2325.
- [4] C. Zweben, B.W. Rosen, *J. Mech. Phys. Solids* 18 (1970) 189.
- [5] A.S. Argon, *Treatise on Materials Science and Technology*, Academic Press, New York, 1972.
- [6] A.S. Argon, in: L.J. Broutman, R.H. Krock (Eds.), *Composite Materials: Fracture and Fatigue*, Academic Press, New York, 1974.
- [7] S.B. Batdorf, *J. Rein. Plast. Comp.* (1982) 153.
- [8] D.G. Harlow, S.L. Phoenix, *J. Comp. Mater.* 12 (1978) 195.
- [9] D.G. Harlow, S.L. Phoenix, *J. Comp. Mater.* 12 (1978) 314.
- [10] S.L. Phoenix, L.J. Tierney, *Eng. Fract. Mech* 18 (1983) 193.
- [11] S.L. Phoenix, P. Schwartz, H.H. Robinson IV, *Comp. Sci. Technol.* 32 (1988) 81.
- [12] R.L. Smith, S.L. Phoenix, M.R. Greenfield, R.B. Henstenburg, R.E. Pitt, *Proc. R. Soc. Lond. A* 388 (1983) 353.
- [13] D.G. Harlow, *Reliability Engineering and System Safety* 56 (1997) 197.
- [14] J.M. Hedgepeth, P. Van Dyke, *J. Compos. Mater.* 1 (1967) 294.
- [15] L. Monette, M.P. Anderson, *Modelling Simul. Mater. Sci. Eng.* 2(1) (1994) 53.
- [16] S.L. Phoenix, I.J. Beyerlein, A.M. Sastry, *Int. J. Solids Structures* 33 (1996) 2543.
- [17] I.J. Beyerlein, S.L. Phoenix, *J. Mech. Phys. Solids* 44 (1997) 2039.
- [18] I.J. Beyerlein, S.L. Phoenix, R. Raj, *Int. J. Solids Structures* 35 (1998) 3177.
- [19] S.J. Zhou, W.A. Curtin, *Acta Metall. Mater.* 8 (1995) 3093.

- [20] P.W. Manders, M.G. Bader, T.W. Chou, *Fibre Sci. Technol.* 17 (1982) 183.
- [21] S. Ochiai, K. Osamura, *J. Mater. Sci.* 23 (1988) 886.
- [22] K. Goda, S.L. Phoenix, *Comp. Sci. Technol.* 50 (1994) 457.
- [23] C. Baxevanakis, D. Jeulin, J. Renar, *Int. J. Fract.* 73 (1995) 149.
- [24] I.J. Beyerlein, S.L. Phoenix, *Eng. Fract. Mech.* 57 (1997) 241.
- [25] I.J. Beyerlein, S.L. Phoenix, *Eng. Fract. Mech.* 57 (1997) 267.
- [26] M. Ibnabdeljalil, W.A. Curtin, *Int. J. Solids Structures* 34 (1997) 2649.
- [27] M. Ibnabdeljalil, W.A. Curtin, *Acta Mater.* 45 (1997) 3641.
- [28] C.M. Landis, I.J. Beyerlein, R.M. McMeeking, Micromechanical simulation of the failure of fiber reinforced composites, *J. Phys. Mech. Solids*, Submitted.
- [29] S.L. Phoenix, I.J. Beyerlein, Strength distributions and size effects in a 1d fracture model for materials under localized stress redistribution among elements, *Phys. Rev. B*, 1998, Submitted.
- [30] W.I. Newman, A.M. Gabrielov, T.A. Durand, S.L. Phoenix, D.L. Turcotte, *Physica D* 77 (1994) 200.
- [31] Y.S. Li, P.M. Duxbury, *Phys. Rev. B* 40(7) (1989) 4889.
- [32] P.M. Duxbury, P.L. Leath, *J. Phys. A: Math. Gen.* 20 (1987) L411.
- [33] P.M. Duxbury, *Statistical Models for the Fracture of Disordered Media*, North Holland, 1990, pp. 189–229.
- [34] I.J. Beyerlein, S.L. Phoenix, *Comp. Sci. Technol.* 56 (1996) 75.
- [35] F.W. Zok, X. Chen, C.H. Weber, *J. Am. Ceram. Soc.* 78 (1995) 1965.
- [36] S.L. Phoenix, C.-Y. Hui, D. Shia, *Comp. Sci. Technol.* 57 (1997) 1707.
- [37] J.M. Hedgepeth, Technical Report NASA TN D-882, NASA, 1961.
- [38] H. Suemasu, *Trans. JSCM* 8 (1982) 29.
- [39] A.M. Sastry, S.L. Phoenix, *SAMPE J.* 30 (1994) 61.
- [40] A. Kelly, *Proc. R. Soc. Lond. A* 319 (1970) 95.